An Optimized Swinging Door Algorithm for Identifying Wind Ramping Events

Mingjian Cui, *Student Member, IEEE*, Jie Zhang, *Senior Member, IEEE*, Anthony R. Florita, *Member, IEEE*, Bri-Mathias Hodge, *Member, IEEE*, Deping Ke, and Yuanzhang Sun, *Senior Member, IEEE*

***Abstract*—With the increasing penetration of renewable energy in recent years, wind power ramp events (WPREs) have started affecting the economic and reliable operation of power grids. In this paper, we develop an optimized swinging door algorithm (OpSDA) to improve the state of the art in WPREs detection. The swinging door algorithm (SDA) is utilized to segregate wind power data through a piecewise linear approximation. A dynamic programming algorithm is performed to optimize the segments by: 1) merging adjacent segments with the same ramp changing direction; 2) handling wind power bumps; and 3) postprocessing insignificant-ramps intervals. Measured wind power data from two case studies are utilized to evaluate the performance of the proposed OpSDA. Results show that the OpSDA provides 1) significantly better performance than the SDA and 2) equal-to-better performance compared to the L1-Ramp Detect with Sliding Window (L1-SW) method with significantly less computational time.**

***Index Terms*—Dynamic programming, sliding window, wind power ramp events (WPREs), swinging door algorithm (SDA).**

NOMENCLATURE

J	Objective function.
$S(i,\ j)$	Score function of the time interval $(i,\ j)$.
$R(i,\ j)$	WPRE rule sets of the time interval $(i,\ j)$.
$B(i,\ j)$	Bump rule sets of the time interval $(i,\ j)$.
Θ	Time interval set of WPREs and non-WPREs.
ξ	Time interval set of WPREs.
$\overline{\xi}$	Time interval set of non-WPREs.
ξ^*	Time interval set of all WPREs.
β	Time interval set of bumps.
η	Time interval set of insignificant-ramps.
η_ξ	Time interval set of WPREs in η.
$\overline{\eta_\xi}$	Time interval set of non-WPREs in η.
$E_{(\cdot)}$	Time interval of WPRE.
$\overline{E_{(\cdot)}}$	Time interval of non-WPRE.
$\overline{E_{(\cdot),\mathrm{b}}}$	Time interval of bump.
$\overline{E_{(\cdot),\eta}}$	Time interval of WPRE in η.
p_t	Wind power values at time t.
$s_{(\cdot)}$	Start time of WPRE.
$e_{(\cdot)}$	End time of WPRE.
$\overline{s_{(\cdot)}}$	Start time of non-WPRE.
$\overline{e_{(\cdot)}}$	End time of non-WPRE.
$\overline{s_{(\cdot),\mathrm{b}}}$	Start time of bump.
$\overline{e_{(\cdot),\mathrm{b}}}$	End time of bump.
$\overline{s_{(\cdot),\eta}}$	Start time of WPRE in η.
$\overline{e_{(\cdot),\eta}}$	end time of WPRE in η.
m	Index of the mth WPRE.
n	Index of the nth non-WPRE as a bump.
v	Index of the vth insignificant-ramps interval.
L	Number of wind power data.
M	Number of WPREs.
N	Number of bumps.
V	Number of WPREs in η.
Q	Number of sliding windows.
ε	Only tunable parameter in the SDA.
λ	Penalty parameter in the L1-SW.
γ	Second derivative threshold in the L1-SW.

Manuscript received April 21, 2015; revised July 13, 2015 and August 24, 2015; accepted September 02, 2015. Date of publication October 07, 2015; date of current version December 11, 2015. This work was supported by the U.S. Department of Energy under Contract DE-AC36-08-GO28308 with the National Renewable Energy Laboratory, in part by the National Basic Research Program of China under Grant 2012CB215101, and in part by the National Natural Science Foundation of China under Grant 51107090. Paper no. TSTE-00343-2015.

M. Cui, D. Ke, and Y. Sun are with the School of Electrical Engineering, Wuhan University, Wuhan 430072, China (e-mail: mj_cui@whu.edu.cn; kedeping@whu.edu.cn; yzsun@mail.tsinghua.edu.cn).

J. Zhang, A. R. Florita, and B.-M. Hodge are with the National Renewable Energy Laboratory (NREL), Golden, CO 80401 USA (e-mail: jie.zhang@nrel.gov; anthony.florita@nrel.gov; bri.mathias.hodge@nrel.gov).

Color versions of one or more of the figures in this paper are available online at http://ieeexplore.ieee.org.

Digital Object Identifier 10.1109/TSTE.2015.2477244

I. INTRODUCTION

LARGE fluctuations in a short time period make wind power generation uncertain, variable, intermittent, and random [1], [2]. This phenomenon, called wind power ramp event (WPRE), sharply threatens the reliable and economic operations of power systems, especially with high wind penetrations [3]. WPREs make it necessary to regulate the output of traditional generators when managing and dispatching the wind power [4]. Therefore, better forecasting and detecting of ramp events [5], [6] are very helpful for power system operators to make operational decisions.

An optimized swinging door algorithm (OpSDA) is developed in this paper to improve the state of the art in WPREs detection. The OpSDA method adopts the optimization concept (through dynamic programming) used in a WPREs detection method recently developed by Sevlian and Rajagopal [7], [8], referred to as the L1-Ramp Detect with Sliding Window (L1-SW). The L1-SW method can characterize the ramp magnitudes, start times, durations, change rates, and other key features needed in the operation of a power system. The L1-SW is capable of smoothing the noise in wind power and

subsequently segregating the wind power into piecewise data. Identified WPREs are then found by a recursion based on dynamic programming algorithm.

The SDA has been used in the literature for ramp forecasting. It was originally proposed by Bristol [9] for data compression and recently used in the renewable energy community. Florita *et al.* [10] applied the SDA to identify variable generation ramp events from historical wind and solar power data. Zhang *et al.* [11] adopted the SDA to extract ramp events from measured and forecasted wind power and evaluate the performance of improved short-term wind power forecasts. Makarov and Ma *et al.* [12]–[15] used the SDA to derive three parameters for each power interval: ramping capability, rate, and duration.

The SDA has been shown to successfully extract WPREs. However, there are still issues in the SDA, such as 1) how to optimally determine the tunable parameter in the SDA, and 2) how to optimally segregate the wind power signal. To address these challenges, we develop an OpSDA method that significantly enhances the performance of the SDA in wind power ramp forecasting.

This paper is organized as follows. The development of the OpSDA is presented in Section II. The experimental results of two case studies are discussed in Section III. In Section IV, the proposed OpSDA is used as a baseline to determine the initial selection of the optimal parameter value in the SDA. Section V concludes this paper.

II. Optimized Swinging Door Algorithm

A. Swinging Door Algorithm

The SDA algorithm [9], [16] is based on the concept of a "swinging door" with a "hinge" or "pivot point" whenever the next point in the time series causes any intermediate point to fall outside the area partitioned by the up and down segment bounds. The segment bounds are defined by the door width $\pm\varepsilon$, which is the only tunable parameter in the SDA. More detailed descriptions of the SDA can be found in [10] and [12]. After segregating the wind power signal by SDA, WPREs are extracted according to the user-specified definition of a significant ramp.

Fig. 1 shows one example of wind power ramp detection results by the SDA. There should be one significant up-ramp (20th h to 28th h) and one significant down-ramp (28th h to 40th h) rather than two up-ramps and three down-ramps, as would be detected using a suboptimal door width value ε. Similar observations can also be seen from the 50th h to 60th h. This phenomenon motivates the development of an optimized SDA, which is capable of combining adjacent up-ramps (or down-ramps) to improve the SDA.

B. OpSDA Based on a Dynamic Programming Approach

The objective of the optimization in the SDA is to minimize the number of individual ramps while still approximating the wind power signal as a ramp [17]. Therefore, adjacent segments that have the same slope (e.g., up-ramps) can be merged into one segment. Toward this end, an optimization process

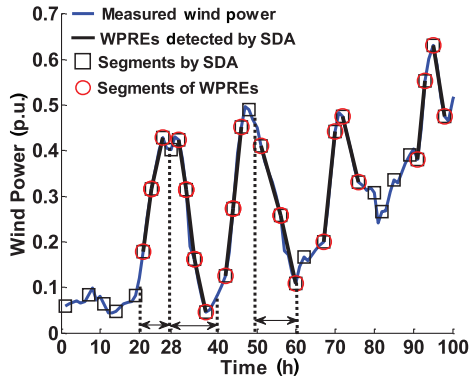

Fig. 1. SDA for wind power ramp detection [10].

is applied to the original segments (from the SDA) using a dynamic programming algorithm. Dynamic programming is a method for solving a complex problem by breaking it down into a collection of simpler subproblems. Every subinterval (subproblem) of the ramp detection problem complies with the same ramp rules. First, the subintervals that satisfy the ramp rules are rewarded by a score function; otherwise, their score is set to zero. Next, the current subinterval is retested as above after being combined with the next subinterval. This process is performed recursively to the end of the dataset. Finally, the significant ramp with the maximum score is extracted. More detailed formulations of the dynamic programming algorithm used in this work are shown in (1)–(13).

In this study, an increasing length score function S is designed based on the length of the interval segregated by the SDA. The optimization problem seeks to maximize the length score function, which corresponds to a ramp event. Given a time interval $(i,\ j)$ of all discrete time points and an objective function J of the dynamic programming algorithm, a WPRE is detected by maximizing the objective function

$$J(i,j) = \max_{i<k\le j} \left[S(i,k) + J(k,j)\right], \quad i<j \tag{1}$$

s.t.

$$S(i,j) > S(i,k) + S(k+1,j) \quad \forall i<k<j \tag{2}$$

$$S(i,j) = (j-i)^2 \times R(i,j) \tag{3}$$

where $J(i,\ j)$ can be computed as the maximum over $(j-i)$ subproblems. The term of $S(i,\ k)$ is a positive score value corresponding to the interval $(i,\ k)$, which conforms to a super-additivity property in (2). There is a family of score functions satisfying (2), and the score function presented in [7] is adopted in this research, expressed as (3). The term $R(i,\ j)$ represents a ramp within the time interval $(i,\ j)$ [18]–[21]. Significant wind power ramps can be defined based on the power change magnitude, direction, and duration. Three definitions proposed in [11] are investigated in this research.

1) *Significant Ramp Definition 1*: The change in wind power output is greater than 20% of the installed wind capacity without constraining the ramping duration.
2) *Significant Ramp Definition 2*: The change in wind power output is greater than 20% of the installed wind capacity within a time span of 4 h or less.

3) *Significant Ramp Definition 3*: A significant up-ramp is defined as the change in wind power output greater than 20% of wind capacity within a time span of 4 h or less; a significant down-ramp is defined as the change in wind power output greater than 15% of the installed wind power capacity within a time span of 4 h or less.

If $R(i,\ j)$ conforms to the threshold of ramp definitions, $R(i,\ j)$ is 1; otherwise, $R(i,\ j)$ is 0. Since the process of detecting down-ramps is the opposite process of detecting up-ramps, note that up-ramp detection is taken as an example to illustrate the specific detecting process.

When optimizing ramps, one of the more interesting findings was the presence of small ramps (non-WPREs), which are termed "bumps" in this paper and set as $B(i,\ j)$ in the formulations below. The key characteristic of a bump is the changing direction (e.g., a down-bump between two up-ramps, or an up-bump between two down-ramps), which makes the iteration of the dynamic programming break abruptly due to the strict super-additivity property in (2). When a bump occurs, it breaks one integrated WPRE into two discrete ramps, which affects the performance of WPREs detection. To address this issue, the dynamic programming process is improved so that it can also merge ramps and bumps with different changing directions. If $B(i,\ j)$ conforms to the threshold of bump definitions, $B(i,\ j)$ is assigned to be 1; otherwise, $B(i,\ j)$ is assigned to be 0. During the recursion, bumps are also considered and merged into the WPRE. The score function in (3) is improved on condition that

$$\forall i \le k < j : [p_{k+1} - p_k] \times [1 - B(k, k+1)] \ge 0. \quad (4)$$

Given a bump interval set $\beta = \{\overline{E_{1,\mathrm{b}}}, \ldots, \overline{E_{N,\mathrm{b}}}\}$, it is a set of intervals, $\overline{E_{n,\mathrm{b}}} = (\overline{s_{n,\mathrm{b}}},\ \overline{e_{n,\mathrm{b}}})$, constructed from the n th non-WPRE interval $\overline{E_n}$, where $\forall\,(s_n, e_n)$, $(s_{n+1}, e_{n+1}) \in \xi$:$1 \le_n$, $e_{n+1} < L$, and $(\overline{s_{n,\mathrm{b}}},\ \overline{e_{n,\mathrm{b}}}) = (e_n + 1,\ s_{n+1} - 1)$. Then, a wind power series with the bump can be depicted as $\Theta = \{\ldots, E_n, \overline{E_{n,\mathrm{b}}}, E_{n+1}, \ldots, E_M, \overline{E_M}\}$. The solution is compressed after combining the two WPREs, E_n and E_{n+1}, around one bump $\overline{E_{n,\mathrm{b}}}$ in (5). Thus, the total number of WPREs decreases to $M - N$

$$(s_n, e_n) \leftarrow (s_n, e_{n+1}). \quad (5)$$

Based on (1)–(5), the optimization process can proceed recursively as follows. Assuming that the number of WPREs is M ($\forall m\colon 1 \le m < M$), the WPRE interval set $\xi = \{E_m, \ldots, E_M\}$ is the set of intervals, $E_m = (s_m,\ e_m)$; and the non-WPRE interval set $\bar{\xi} = \{\overline{E_m}, \ldots, \overline{E_M}\}$ is the set of intervals $\overline{E_m} = (\overline{s_m},\ \overline{e_m})$. If $\forall(\overline{s_m}, \overline{e_m}) \in \bar{\xi}$ and $\forall i, j :\ \overline{s_m} < i < j < \overline{e_m}$, then

$$\begin{aligned} R(i,j) &= 0 \\ S(i,j) &= 0 \\ J^*(\overline{s_m}, \overline{e_m}) &= 0. \end{aligned} \quad (6)$$

If $\forall\,(s_m, e_m) \in \xi$ and $\forall i, j : s_m < i < j < e_m$, the objective function $J^*(s_m, e_m)$ is set as

$$\begin{aligned} J^*(s_m, e_m) &= \max_{s_m < k_1 < e_m} [S(s_m, k_1) + J(k_1 + 1, e_m)] \\ &= \max_{s_m < k_1 < e_m} S(s_m, k_1) + \max_{k_1+1 < k_2 < e_m} S(k_1+1, k_2) \\ &\quad + \cdots + \max_{k_{i-1}+1 < k_i < e_m} S(k_{i-1}, k_i) \\ &\quad + J(k_i + 1, e_m) \\ &= \max_{s_m < k_1 < k_2 < \cdots < k_{i-1} < k_i < e_m} S(s_m, k_1) \\ &\quad + S(k_1 + 1, k_2) + \cdots + S(k_{i-1}, k_i). \end{aligned} \quad (7)$$

Thus, considering (2), $J^*(s_m, e_m)$ equals $S(s_m,\ e_m)$. An optimal event sequence of WPREs and non-WPREs can be presented as $\Theta = \{E_m, \overline{E_m}, E_{m+1}, \overline{E_{m+1}}, \ldots, E_M, \overline{E_M}\}$ or $\{E_m, E_{m+1}, \overline{E_{m+1}}, \ldots, E_M, \overline{E_M}\}$, for a given wind

$$\begin{aligned} J^*(s_m, \overline{e_M}) &= \max_{s_m < k_1 \le e_m} [S(s_m, k_1) + J(k_1 + 1, \overline{e_M})] \\ &= \max_{s_m < k_1 \le e_m} \left\{ S(s_m, k_1) + \max_{k_1+1 < k_2 \le e_m} [S(k_1 + 1, k_2) + J(k_2 + 1, \overline{e_M})] \right\} \\ &= \max_{s_m < k_1 \le e_m} \left\{ S(s_m, k_1) + \max_{k_1+1 < k_2 \le e_m} \left\{ S(k_1 + 1, k_2) + \cdots + \max_{k_{i-1}+1 < k_i \le e_m} [S(k_{i-1}, k_i) + J(k_i + 1, \overline{e_M})] \right\} \right\} \\ &= \max_{s_m < k_1 < k_2 < \cdots < k_{i-1} < k_i \le e_m} [S(s_m, k_1) + S(k_1 + 1, k_2) + \cdots + S(k_{i-1}, k_i)] + \max_{k_{i-1}+1 < k_i \le e_m} J(k_i + 1, \overline{e_M}) \end{aligned} \quad (8)$$

$$\begin{aligned} J^*(\overline{s_m}, \overline{e_M}) &= \max_{\overline{s_m} < k_1 \le \overline{e_m}} [S(\overline{s_m}, k_1) + J(k_1 + 1, \overline{e_M})] \\ &= \max_{\overline{s_m} < k_1 \le \overline{e_m}} \left\{ S(\overline{s_m}, k_1) + \max_{k_1+1 < k_2 \le \overline{e_m}} [S(k_1 + 1, k_2) + J(k_2 + 1, \overline{e_M})] \right\} \\ &= \max_{\overline{s_m} < k_1 \le \overline{e_m}} \left\{ S(\overline{s_m}, k_1) + \max_{k_1+1 < k_2 \le \overline{e_m}} \left\{ S(k_1 + 1, k_2) + \cdots + \max_{k_{i-1}+1 < k_i \le \overline{e_m}} [S(k_{i-1}, k_i) + J(k_i + 1, \overline{e_M})] \right\} \right\} \\ &= \max_{\overline{s_m} < k_1 < k_2 < \cdots < k_{i-1} < k_i \le \overline{e_m}} [S(\overline{s_m}, k_1) + S(k_1 + 1, k_2) + \cdots + S(k_{i-1}, k_i)] + \max_{k_{i-1}+1 < k_i \le \overline{e_m}} J(k_i + 1, \overline{e_M}). \end{aligned} \quad (9)$$

power series with L values. If a wind power series, $p_{s_m}, \ldots, p_{\overline{e_M}}$, with the event sequence, $\Theta = \{E_m, \overline{E_m}, E_{m+1}, \overline{E_{m+1}}, \ldots, E_M, \overline{E_M}\}$, has a solution to (1) being $J^*(s_m, \overline{e_M})$, the solution is shown in (8), shown at the bottom of the previous page, and (10). If a wind power series $p_{s_m}, \ldots, p_{\overline{e_M}}$, with the event sequence $\Theta = \{E_m, E_{m+1}, \overline{E_{m+1}}, \ldots, E_M, \overline{E_M}\}$, has a solution to (1) being $J^*(\overline{s_m}, \overline{e_M})$, the solution is shown in (9), shown at the bottom of the previous page, and (11).

Thus, considering (2), $J^*(s_m, \overline{e_M})$ in (8) can be transformed to

$$J^*(s_m, \overline{e_M}) = S(s_m, e_m) + J^*(\overline{s_m}, \overline{e_M}). \tag{10}$$

Likewise, considering (6), $J^*(\overline{s_m}, \overline{e_M})$ in (9) can be transformed to

$$\begin{aligned} J^*(\overline{s_m}, \overline{e_M}) &= \max_{\overline{s_m} < k_1 < k_2 < \cdots < k_{i-1} < k_i \le \overline{e_m}} J(k_i + 1, \overline{e_M}) \\ &= J^*(s_{m+1}, \overline{e_M}). \end{aligned} \tag{11}$$

If a wind power series is $p_{s_1}, \ldots, p_{\overline{e_M}}$, the solution is

$$J^*(s_1, \overline{e_M}) = \sum_{m=1}^{M} S(s_m, e_m). \tag{12}$$

If a wind power series is $p_{\overline{s_1}}, \ldots, p_{\overline{e_M}}$, the solution is

$$J^*(\overline{s_1}, \overline{e_M}) = \sum_{m=2}^{M} S(s_m, e_m). \tag{13}$$

This process is implemented and modified based on the algorithm developed in [7], which is given in Algorithm 1 with pseudocode. The main contribution in Algorithm 1 (compared to [7]) is the introduction of an improved score function based on (4) to merge bumps into one WPRE.

C. Insignificant-Ramps Postprocessing

Another interesting finding in ramp detection is the appearance of WPRE within a set of the highly frequent "insignificant-ramps." The "insignificant-ramps" interval set is defined as an interval with a high occurring frequency of up- and down-ramps having smaller magnitudes. A WPRE may appear in the insignificant-ramps interval after smoothing the wind power signal within the interval. Given a WPREs' interval set $\eta_\xi = \{\overline{E_{1,\eta}}, \ldots, \overline{E_{V,\eta}}\}$ detected in the insignificant-ramps intervals, it is a set of intervals $\overline{E_{v,\eta}} = (\overline{s_{v,\eta}}, \overline{e_{v,\eta}})$ constructed from the vth non-WPRE interval $\overline{E_v}$ $(\overline{E_{v,\eta}} \in \overline{E_v})$ where $\forall\,(s_v, e_v)\,,\ (s_{v+1}, e_{v+1}) \in \xi:\ 1 \le s_v, e_{v+1} < L$, and $e_v \le \overline{s_{v,\eta}} < \overline{e_{v,\eta}} \le s_{v+1}$. The solution $J^*(s_1, \overline{e_M})$ in (12) and $J^*(\overline{s_1}, \overline{e_M})$ in (13) is extended with $\overline{E_{v,\eta}}$. Now, the total number of WPREs increases to $M - N + V$.

To detect WPREs in the insignificant-ramps interval, a postprocessing procedure is implemented to find the difference between the maximum and minimum wind power within the interval

$$\{\max[p_{e_v},\ p_{s_{v+1}}] - \min[p_{e_v},\ p_{s_{v+1}}]\} \in R \tag{14}$$

where $\overline{s_{v,\eta}}$ and $\overline{e_{v,\eta}}$ are the time points corresponding to the maximum and minimum values within the time interval $[e_v,\ s_{v+1}]$, respectively. R is the ramp definition given in (3).

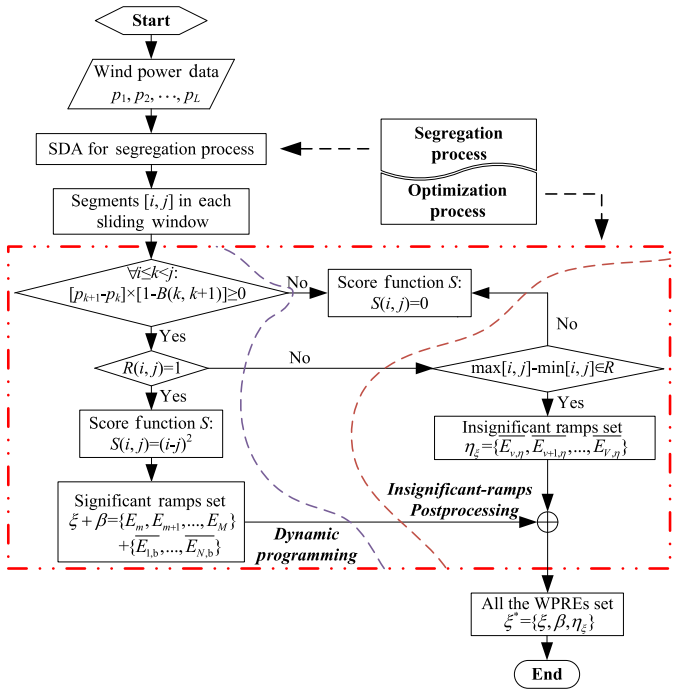

Fig. 2. Overall flowchart of detecting WPREs.

Algorithm 1. Modified Dynamic Programming Pseudocode Based on [7] and [8]

```
//Length of ramp segments by the SDA.
L ← length(p)
// Initialize scores of zero length segments.
for i = 1 → L do
   J[i, i] ← 0
end for
// Compute maximum scores for combined segments.
for n = 2 → L do
  for i = 1 → L − n + 1 do
     j ← i + n − 1
  for k = i → j − 1 do
    // Process bumps
    for kk = i → k
      if [p_{kk+1} − p_{kk}] × [1 − B(kk, kk + 1)] ≥ 0 then
        S(i, k) ← (k − i)^2 × R (i, k)
      else then
        S(i, k) ←0
        break for
      end if
    end for
    q ← S(i, k) + J(k, j)
    if q < J[i, j] then
      J[i, j] ← q
      K[k, j] ← k
    end if
  end for
 end for
end for
```

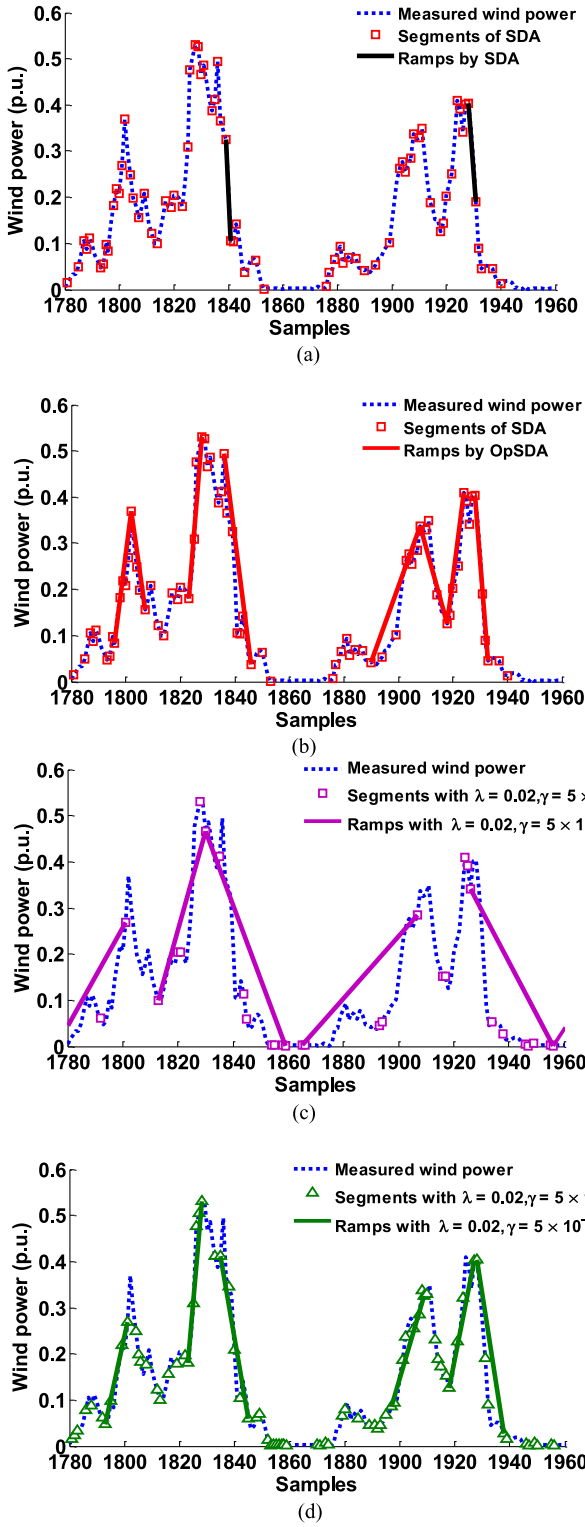

Fig. 3. Comparison of results for detection performance of the SDA, L1-SW, and OpSDA. (a) Detection performance comparisons of the SDA, and (b) OpSDA with $\varepsilon = 9 \times 10^{-3}$. (c) Detection performance of the L1-SW with larger $\lambda = 0.5$, $\gamma = 1 \times 10^{-4}$, and (d) smaller $\lambda = 0.02$, $\gamma = 5 \times 10^{-6}$.

D. Procedure of Detecting WPREs Using the OpSDA

The relationship of WPREs, bumps, and insignificant-ramps is expressed as $\Theta = \{\xi,\ \bar{\xi}\}, \bar{\xi} = \{\beta,\ \eta,\ \overline{\beta + \eta}\}, \eta = \{\eta_\xi,\ \overline{\eta_\xi}\}$, and $\xi^* = \xi + \beta + \eta_\xi$, in which ξ^* is the eventually optimal solution with $(M - N + V)$ WPREs. The overall flowchart of detecting WPREs is shown in Fig. 2.

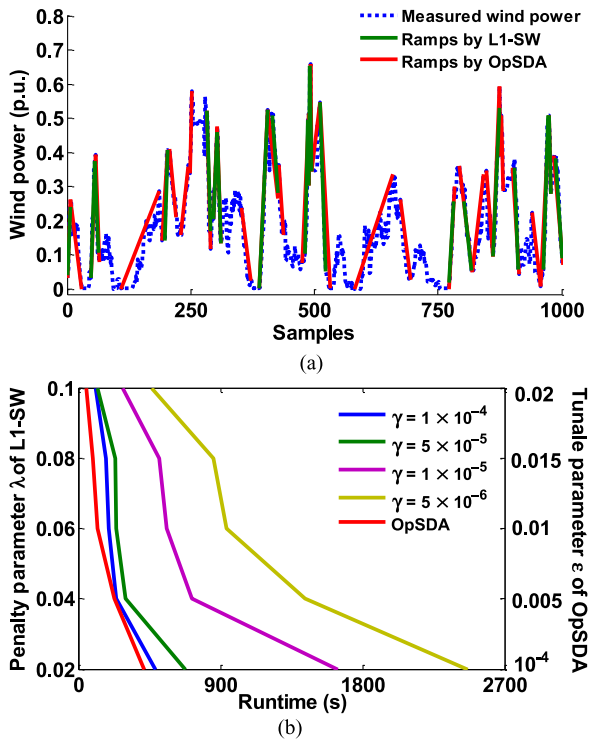

Fig. 4. (a) Sample results (the first 1000 points) of ramp detection in the 1-year wind power data. (b) Runtime comparison of the L1-SW with the parameters $\lambda \in [0.02, 0.1]$, $\gamma = [1 \times 10^{-4}, 5 \times 10^{-5}, 1 \times 10^{-5}, 5 \times 10^{-6}]$ to the OpSDA with $\varepsilon \in [0.0001, 0.02]$.

In Fig. 2, $p_1, p_2, \ldots, p_L$ is a set of measured wind power data. There are Q sliding windows with the start point $(t_{\text{ws}}, p_{\text{ws}})$ and the end point $(t_{\text{we}}, p_{\text{we}})$, parameterized by window length WL and window overlap WO. The start and end points of the ith window are given by the following equations:

$$t_{\text{ws},i} = (i-1) \times (\text{WL} - \text{WO}), i \in Q \tag{15}$$

$$t_{\text{we},i} = i \times \text{WL} - (i-1) \times \text{WO}, i \in Q. \tag{16}$$

In brief, all segments (represented by the square points in Fig. 1) are first extracted by the SDA with a predefined parameter ε. These segments are input into the dynamic programming algorithm (within the left part of the red block shown in Fig. 2) to merge ramps and bumps. Then, postprocessing (within the right part of the red block shown in Fig. 2) is performed to extract the WPREs occurring in the insignificant-ramps interval sets. Eventually, the set of optimized significant ramp events $\xi^* = \{(s_1, e_1), \ldots, (s_L, e_L)\}$ is identified.

III. Experimental Results

In this section, the OpSDA is applied to two case studies. We present various statistics to analyze the detected WPREs and parameterize the WPRE process.

1) Case I: We analyze a time series of measured wind power production from a wind site in Qiaowan, Gansu, China. The dataset contains 34 818 samples representing

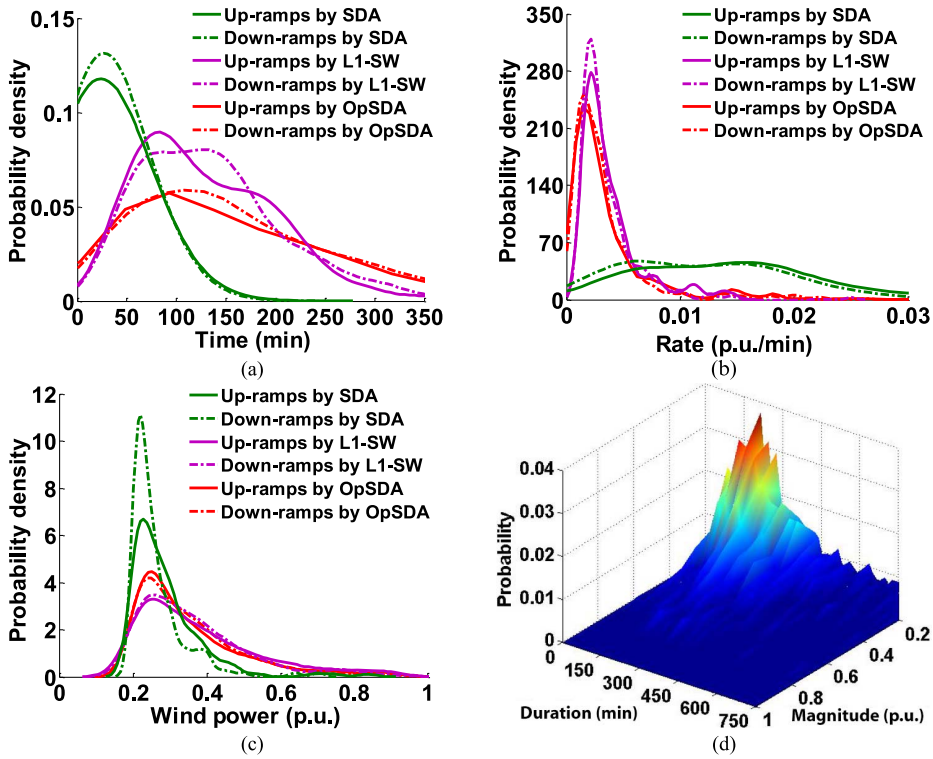

Fig. 5. Probability density distributions of the ramp features for up-ramps and down-ramps detected by the L1-SW, SDA, and OpSDA. (a)–(c) Distributions of ramp duration, ramp change rate, and ramp magnitude, respectively. (d) Visualized joint distribution of ramp durations and magnitudes detected by the OpSDA (3-D probabilities of ramp features)

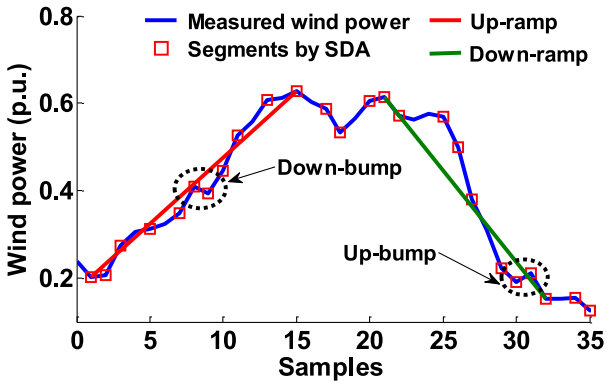

Fig. 6. Sample interval of two wind power bumps.

measured wind power output sampled every 15 min. These data represent wind power data spanning from January 1, 2013, to December 31, 2013, at a plant with 201 MW of capacity.

2) Case II: The second case is the total wind power generation taken from a balancing area in the northwestern region of the USA. The dataset contains 7 884 012 samples sampled every 4 s spanning from October 1, 2012, to September 30, 2013. In this case, we use the maximum power output 123 MW as the base benchmark capacity.

Case I is focused on evaluating the performance of the OpSDA by comparing the detection behavior of three methods: L1-SW, SDA, and OpSDA. Case II is focused on statistical analysis of different timescales of ramp detections, considering the high resolution of the dataset.

A. Case I: Specific Ramps Comparison of the SDA, L1-SW, and OpSDA

In this section, Definition 1 defined in Section II-B is adopted. A significant ramp is defined as the change in wind power that is greater than 20% of the installed wind capacity. Note that this threshold (20%) is set relatively small to extract sufficient ramps to compare the SDA, L1-SW, and OpSDA. It is also important to note that we do not attempt to solve the optimal tunable parameters in L1-SW, which is planned in future work.

Fig. 3 compares the significant ramps extracted by the three methods: L1-SW, SDA, and OpSDA. Figs. 3(a) and (b) compare the segments and ramps approximated by the SDA to that by the OpSDA with the same parameter value ε (9×10^{-3}). Figs. 3(c) and (d) illustrate the segments and ramps approximated by the L1-SW with different parameter values [larger values: $\lambda = 0.5, \gamma = 1 \times 10^{-4}$ in Fig. 3(c); and smaller values: $\lambda = 0.02, \gamma = 5 \times 10^{-6}$ in Fig. 3(d)]. Corresponding segments of significant ramps are also shown in these two subfigures.

Figs. 3(a) and (b) show that many segments are extracted by the SDA with a relatively small ε. Without any optimization and combination, the SDA can only detect two WPREs, while the OpSDA can combine insignificant-ramps detected by the SDA into one significant ramp; therefore, eight WPREs are detected by the OpSDA. Figs. 3(c) and (d) indicate that more segments are extracted by the L1-SW with smaller λ and γ than that with larger λ and γ. Smaller parameters λ and γ produce more accurate detection results, but more computation time is consumed because of more iterations for segregation.

TABLE I
STATISTICAL RESULTS OF ESTIMATION METRICS

	L1-SW		OpSDA	
	End (YES)	End (NO)	End (YES)	End (NO)
Start (YES)	149/18%	224/27%	653/65%	151 /14%
Start (NO)	174/21%	283/34%	131/13%	70/8%
Total	830		1005	

TABLE II
NUMBER OF DETECTED SIGNIFICANT RAMPS

Definitions	Methods	Up-ramps	Down-ramps	Total
Def. 1	SDA	135	148	283
	L1-SW	413	417	830
	OpSDA	503	502	1005
Def. 2	SDA	135	148	283
	L1-SW	421	427	848
	OpSDA	511	515	1026
Def. 3	SDA	135	322	457
	L1-SW	421	528	949
	OpSDA	611	684	1295

By comparing all four subfigures in Fig. 3, it is observed that segments of the SDA [red rectangles in Figs. 3(a) and (b)] are more accurate than that of the L1-SW with larger λ and γ [purple rectangles in Fig. 3(c)]. For example, as shown in the interval from points 1860 to 1910, the L1-SW [purple line in Fig. 3(c)] deviates from the measured wind power signal with larger λ and γ. By reducing the values of λ and γ, the L1-SW in Fig. 3(d) (green line) can match the measured wind power signal more precisely. However, comparing Figs. 3(a)–(d), the OpSDA performs better than the L1-SW at sharp-inflection points, such as Points 1802 and 1838. Specifically, the set of metrics in (17) and (18) is proposed to evaluate the detection performance of the OpSDA and L1-SW

$$[p(t+1)-p(t)]\times[p(t)-p(t-1)]<0 \tag{17}$$

where t represents the current time. This formulation of (17) indicates that the start (or end) point of one WPRE, denoted as Start (YES) [or End (YES)], is successfully extracted when the start (or end) point is a sharp-inflection point

$$[p(t+1)-p(t)]\times[p(t)-p(t-1)]>0 \tag{18}$$

where t represents the current time. This formulation of (18) indicates that the start (or end) point of one WPRE, denoted as Start (NO) [or End (NO)], is extracted when the start (or end) point is NOT an inflection point. Table I lists the number of WPREs with Start (YES), End (YES), Start (NO), and End (NO) found by both the OpSDA and L1-SW in the examined dataset. The percentage of total WPREs is also provided.

Table I shows that L1-SW only detects 149 WPREs (18% of total WPREs) with both accurate start and end inflection points. However, the OpSDA detects 653 WPREs (65% of total WPREs) with both accurate start and end inflection points. Moreover, there are only 70 WPREs (8% of total WPREs) that the OpSDA does not accurately detect either the start or end inflection points, whereas there are 283 WPREs (34% of total WPREs) that L1-SW does not accurately detect either the start or end inflection points.

Table II lists the number of significant up- and down-ramps in Case I data of the three methods under three significant ramp definitions, where OpSDA detected more significant ramps than the other two methods for all three definitions.

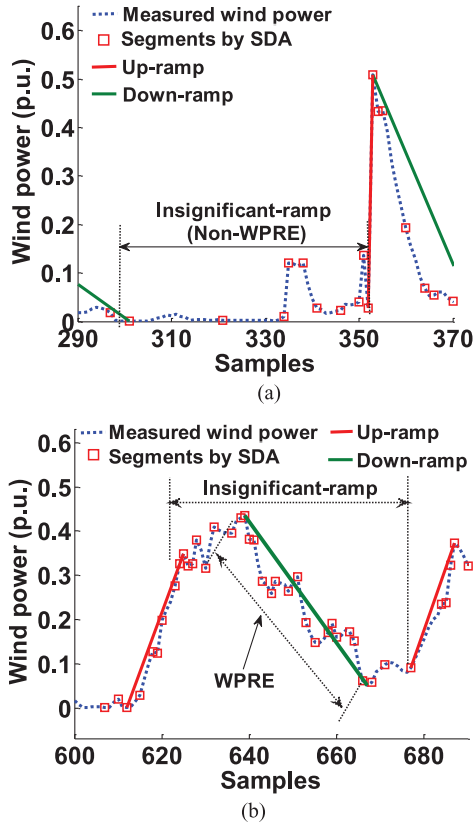

Fig. 7. One sampled non-WPRE and WPRE in the insignificant-ramps interval. (a) Non-WPRE in insignificant-ramps. (b) WPRE in insignificant-ramps.

Fig. 4(a) shows sampled ramps detected within the 1-year period. Fig. 4(b) compares the runtime of the two methods: 1) the L1-SW on the left y-axis, and 2) OpSDA on the right y-axis. Although the detection results in the L1-SW [Fig. 3 (d)] are accurate by visual inspection with smaller λ and γ, the runtime of the L1-SW [Fig. 4(b)] is more than 35 min when λ is 0.02 and γ is 5×10^{-6}; however, the runtime of the OpSDA with ε (9×10^{-3}) is only approximately 3 min. Overall, both the ramp detection performance and the runtime of the L1-SW are very sensitive to the penalty parameter λ and threshold γ, whereas the runtime of the OpSDA is less sensitive to the parameter ε.

Fig. 5 shows the statistical analysis of the three key ramp features (duration, change rate, and magnitude). It is observed that the OpSDA (red lines) and L1-SW (purple lines) have similar empirical distributions of ramp duration, change rate, and magnitude for both the up-ramps and down-ramps. However, the SDA generally has a shorter ramp duration peak of approximately 30 min [with the highest frequency in Fig. 5(a)] without any combination and optimization of segments.

Overall, for detecting and analyzing significant ramps, both the OpSDA and L1-SW (with smaller γ and ε) can characterize the reasonable ramp detection behavior for long-time dispatching problems. And, the OpSDA is more preferable because of its computational efficiency and better performance at the sharp-inflection points.

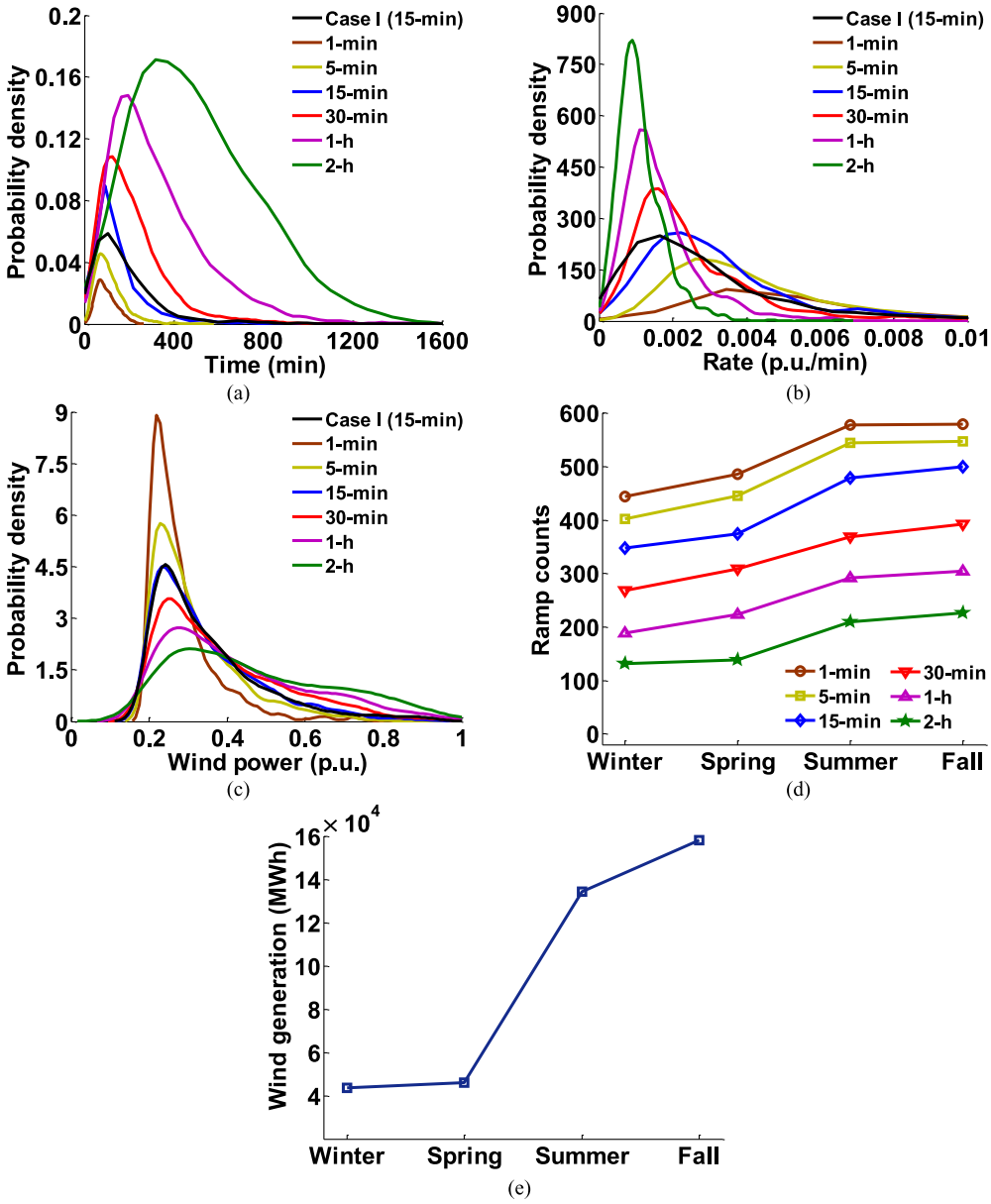

Fig. 8. Probability density distributions of ramp features of six timescales (1-min, 5-min, 15-min, 30-min, 1-h, and 2-h) and seasonal ramp counts over a whole year for Case II. (a) Ramp duration. (b) Ramp change rate. (c) Ramp magnitude. (d) Seasonal ramp counts. (e) Seasonal wind generation.

B. Case I: Bumps and Insignificant-Ramps Performance

There are total 238 bumps that are detected and merged into WPREs. In Fig. 6, one up-bump and one down-bump are shown with very short time durations and small magnitudes. Without considering bumps, the ramp from Point 1 to Point 15 would be cut into two separate and independent sub-WPREs (points 1–8 and points 9–15). This phenomenon seriously affects the ramp detection performance. Note that the ramps detected and analyzed by the OpSDA in Section III-A already merged bumps to the adjacent segments.

The OpSDA has detected 102 WPREs that were not found using the L1-SW or the SDA due to the insignificant-ramps postprocessing procedure (shown in Fig. 2). Two of them (points 301–351 and points 625–675) are shown in Fig. 7. Fig. 7(a) indicates that none of WPREs occurs in the insignificant-ramp interval (points 301–351) due to an approximately flat tendency. Fig. 7(b) shows a down-ramping tendency in the insignificant-ramp interval (points 625–675), which is successfully identified as a WPRE without considering the frequent slight fluctuations.

C. Case II: Ramp Detection at Multiple Timescales

In this section, the OpSDA is used to detect all WPREs in the Case II dataset. The 4-s dataset is averaged to obtain wind power data at different timescales: 1-min, 5-min, 15-min, 30-min, 1-h, and 2-h timescales. A total of 2089 ramps within 1-min timescale (1941 ramps within 5-min timescale, 1701 ramps within 15-min timescale, 1340 ramps within 30-min timescale, 1009 ramps within 1-h timescale, and 705 ramps

within 2-h timescale) are detected and utilized to generate the probability density distributions. Fig. 8 shows the ramp feature statistics and seasonal ramp counts of each timescale over the course of a whole year.

Fig. 8(a) indicates that along with the increasing timescale (from 1-min to 2-h), for ramp durations, the peak duration value and probability density rise from 50 min with 0.03 to 400 min with 0.17. For the distribution of ramp change rate in Fig. 8(b), the peak change rate value decreases from 0.004 to 0.001 p.u./min, whereas the corresponding probability density rises from 80 to 820. For the distribution of ramp magnitude in Fig. 8(c), the peak magnitude value rises from 0.21 to 0.33 p.u., whereas the corresponding probability density decreases from 9 to 2.

Fig. 8(d) illustrates that the seasonal ramp counts also decrease along with the increasing timescale in each season. There are relatively fewer ramp events occurring in winter and spring, whereas more ramp events occur in summer and fall. This can be partially attributed to the higher wind generation in summer and fall as shown in Fig. 8(e). It is seen from Figs. 8(d) and (e) that seasonal ramp counts increase along with the increasing wind generation.

Another interesting finding is the ramp features' comparison at different geographic locations. For the same 15-min timescale, the probability density distributions of ramp features in Case II wind power data (the blue line) are very close to that in the Case I wind power data (the black line), especially the ramp magnitude distribution.

Fig. 9 presents the scatter diagram of the ramp duration and magnitude within two timescales (15-min and 1-h) for up- and down-ramps. For each scatter diagram, all the points are distributed relatively symmetrically between up- and down-ramps for the same timescale. However, by comparing the two timescales in Figs. 9(a) and (b), the points spread along with the increasing timescale. For up-ramps, more points are concentrated around the bottom left corner for the 15-min timescale, whereas more points spread to the top right corner for the 1-h timescale; likewise for down-ramps.

On the other hand, more severe WPREs with larger magnitudes and longer durations are identified within the 1-h timescale [shown in Fig. 9(b)] than that within the 15-min timescale [shown in Fig. 9(a)], which is due to not considering the intra-hour variability because of the hourly averaging. This finding can potentially affect the day-ahead security-constrained unit commitment [22], in which the hourly time resolution is mainly focused on. Under the circumstances, more WPREs could likely present themselves as severe contingencies, which may present challenges for power system operators.

IV. Application of OpSDA for Tuning the ε Parameter

The SDA has the advantage of computational and structural simplicity, which is favorable considering its robustness, even with noisy data [12]. Sometimes the SDA without any optimization is preferable because of its inexpensive computation. However, it is still rare in the literature to discuss how to best

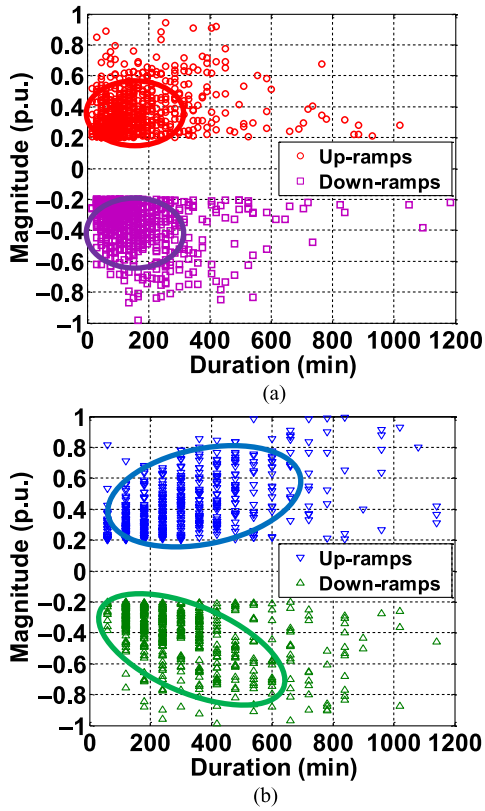

Fig. 9. Scatter diagram of durations and magnitudes for up- and down-ramps within 15-min and 1-h timescales. (a) 15-min timescale. (b) 1-h timescale.

TABLE III
Contingency Table for the SDA and OpSDA

	OpSDA (YES)	OpSDA (NO)	Total
SDA (YES)	TP (*hits*)	FP (*false alarm*)	TP+FP
SDA (NO)	FN (*misses*)	TN	FN+TN
Total	TP+FN	FP+TN	N=TP+FP+FN+TN

set the tunable parameter ε_{opt} when using the SDA [10], [11]. Thus, it would be helpful to develop a framework for adaptively selecting the best ε values. In this research, the proposed OpSDA is used as a baseline to determine the optimal value of the tunable parameter ε_{opt}. The solving procedure is to find the ε_{opt} that enables the ramps detected by the SDA close to that detected by the OpSDA. Generally, with a smaller ε value, the fitting errors between the SDA approximated wind power and the measured wind power will be smaller. However, an ε value that is too small may divide a single significant ramp into multiple small ramps that do not satisfy the WPRE ramp definitions.

To determine the optimal parameter based on the OpSDA, a suite of WPRE detection metrics are used to evaluate the performance of ramp extraction with different ε values. The adopted metrics include the probability of detection (POD), the critical success index (CSI), the frequency bias score (FBIAS), and the success ratio (SR) [11], [23]. They are calculated based on a contingency table in Table III that provides a measure of skill for the SDA approaching the OpSDA. True positive (TP)

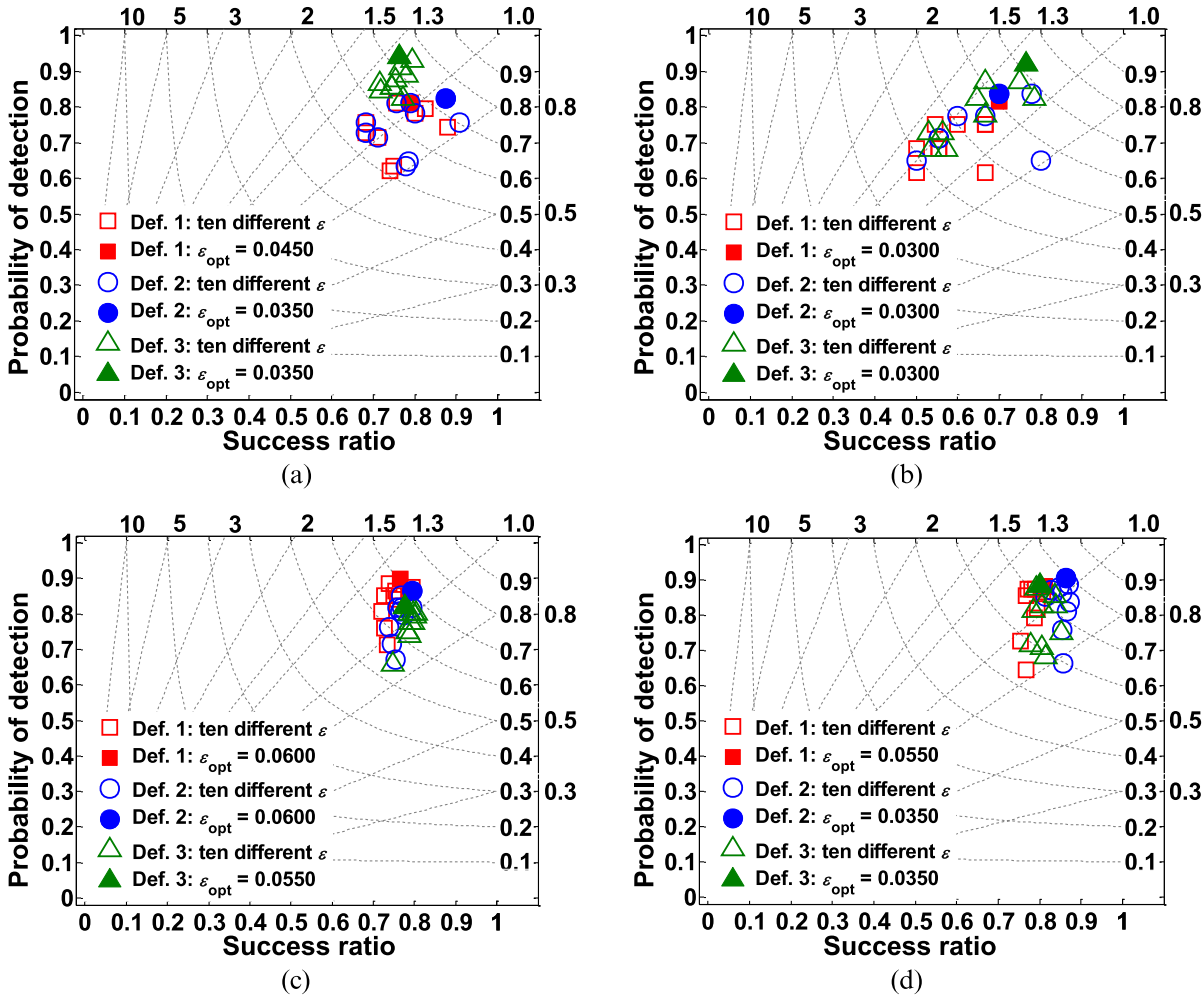

Fig. 10. WPREs detection performance with the optimal parameters. (a)–(d) Optimal parameters defined by three ramp definitions in January, April, July, and October 2013, respectively.

represents the number of ramps detected by the SDA that are also detected by the OpSDA; false positive (FP) is the number of ramps detected by the SDA that are not detected by the OpSDA; false negative (FN) represents the number of ramps detected by the OpSDA that are not extracted by the SDA; true negative (TN) is the number of nonoccurring events for both the SDA and the OpSDA; and N is the total number of WPREs.

After calculating all metrics (POD, CSI, FBIAS, FAR, and SR), the optimal ε value is determined according to the largest POD, which can be visualized on the performance diagram, as shown in Fig. 10. A performance diagram is used to understand the evolution of the SDA with 10 different ε values. For a performance diagram shown in Fig. 10, 1) the left axis represents the value of POD; 2) the bottom axis represents SR; 3) the diagonal dashed lines represent FBIAS; and 4) the dashed curves represent CSI. Fig. 10 shows a performance diagram of 10 ε values by utilizing each ramp definition. These 10 parameters are uniformly derived from 0.002 to 0.065. To find the optimal parameter ε_{opt}, the points in Fig. 10 move toward the top right corner of the performance diagram. Fig. 10 shows the optimal parameters for four months (January, April, July, and October 2013) using 15-min timescale of Case I data based on three significant wind power ramp definitions.

It is observed from Fig. 10 that the optimal parameters have the same values under the three definitions ($\varepsilon_{\text{opt}} = 0.03$) in April. While in January and October, ε_{opt} has the same value in Definitions 2 and 3 ($\varepsilon_{\text{opt}} = 0.035$), whereas in July, it has the same value in Definitions 1 and 2 ($\varepsilon_{\text{opt}} = 0.06$). This indicates that the value of ε_{opt} is generally sensitive to the ramping definition chosen by users. In addition, when using ε_{opt}, both the POD and SR values are larger than 0.7 in the four analyzed months; the FBAIS values are close to 1; and the CSI values are larger than 0.6. This means that the ramp detection results obtained by the SDA with ε_{opt} can reasonably approach the results obtained by the OpSDA. This finding can guide power system operators to make decisions about how to determine the optimal parameter in SDA to best detect WPREs. This process of determining the optimal parameter in the SDA can be implemented by a framework illustrated in Fig. 11. According to the POD, CSI, FBIAS, and SR metrics, the optimal parameter value ε_{opt} can be found by repeating the search process in Fig. 11. Power system operators can use this framework to directly determine the optimal parameter in SDA

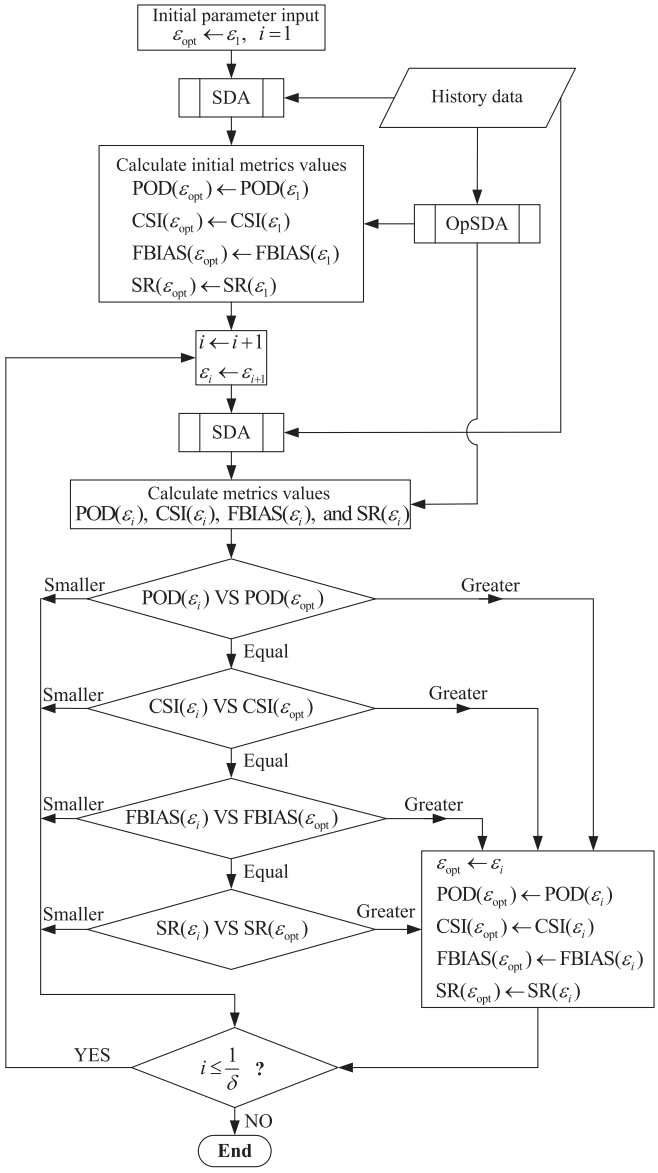

Fig. 11. Flowchart to determine the optimal parameter in the SDA.

for WPREs detection. The initial optimal parameter value is ε_1. The step size of the search process is δ ($\delta = 0.005$ in this paper). Then, the parameter ε_i is expressed as

$$\varepsilon_i = \varepsilon_1 + (i-1) \times \delta \left(0 < i \le \frac{1}{\delta}\right). \tag{19}$$

V. Discussion

The OpSDA method is readily applicable to a variety of cases in power system operations. OpSDA can be used by utilities and independent system operators (ISOs) for wind power ramp forecasting and detection, thereby assessing the impact of wind ramp and forecast uncertainties on the grid's operation in an online fashion. In addition to wind power, OpSDA can also be applied to electric load and other variable and uncertain renewable energy such as solar power [24]. The detected and forecasted ramps (in wind, solar, or load) can be useful for power systems operation functions, such as a flexible ramping product market design.

The results in this paper have shown that the OpSDA can successfully detect WPREs. It is important to note that OpSDA can also be used to provide wind power ramp forecasting. The OpSDA method could be adopted in two ways for wind power ramp forecasting. In the first, the OpSDA can be applied in addition to wind power forecasting methods to forecast wind power ramps. Wind power forecasts can be produced by multiple forecasting methods such as numerical weather predictions, statistical, and machine learning methods. The OpSDA could be adopted in a postprocessing method to detect ramping events in the forecasted wind power. Both deterministic and probabilistic ramp forecasts can be produced in this way. In the second case, OpSDA can be directly applied to historical measured wind power data to extract all historical ramping events. Statistical and machine learning methods will be developed based on the historical ramping events to directly forecast ramping features (e.g., ramping magnitude, duration, and rate) at different timescales.

In addition to wind power, the OpSDA method can also be applied to electric load and other variable and uncertain renewable energy such as solar power. For solar ramp events' detection, OpSDA should be applied to both actual and clear-sky solar power generations. Ramping events occurring in both clear-sky and measured solar powers would be removed. OpSDA can also be used in solar power ramp forecasting in a similar manner to wind power ramp forecasting.

With the increasing penetration of wind and solar power, system operators have observed a lack of system flexibility and ramping capacity in real-time dispatch stages. Several ISOs [25], [26] are implementing new products during the different unit commitment stages to ensure that sufficient ramping is available during real-time operations. With the accurate detection and forecasting of wind and solar power ramp events by OpSDA, wind- and solar-friendly flexible ramping products can be developed. The wind- and solar-friendly flexible ramping products aim to take advantage of the wind and solar power ramps typically known for their negative characteristics.

VI. Conclusion

An OpSDA was developed in this research for wind power ramp detection. The developed OpSDA was compared to the SDA and L1-SW methods in two case studies. The results showed that the OpSDA successfully identified WPREs and performed significantly better than the SDA. The OpSDA also provided equal-to-better performance than the L1-SW with much less computational time. In addition to the direct ramps detection, the OpSDA was also used as a baseline to determine the optimal value of the tunable parameter ε_{opt} in the SDA, which could be performed offline.

This proposed OpSDA method and corresponding results can also be used in unit commitment problems, ramp capability products, and solar power ramps detection, which will be investigated in future work.

ACKNOWLEDGMENT

The authors would like to thank Prof. X. Zha, Wuhan University, China, for his provision of wind power data for Case I.

REFERENCES

[1] P. Sorensen *et al.*, "Power fluctuations from large wind farms," *IEEE Trans. Power Syst.*, vol. 22, no. 3, pp. 958–965, Aug. 2007.
[2] H. Jiang, Y. Zhang, J. J. Zhang, D. W. Gao, and E. Muljadi, "Synchrophasor-based auxiliary controller to enhance the voltage stability of a distribution system with high renewable energy penetration," *IEEE Trans. Smart Grid*, vol. 6, no. 4, pp. 2107–2115, Jul. 2015.
[3] H. Ma and Y. Liu, "An IGDT-based intraday scheduling strategy method considering wind power ramp event," in *Proc. IEEE Power Energy Soc. Gen. Meeting*, Denver, CO, USA, 2015.
[4] J. Freedman, M. Markus, and R. Penc. *Analysis of West Texas Wind Plant Ramp-Up and Ramp-Down Events* [Online]. Available: http://interchange.puc.state.tx.us/WebApp/Interchange/Documents/33672_1014_580034.pdf. 2008.
[5] M. Cui, D. Ke, Y. Sun, D. Gan, J. Zhang, and B.-M. Hodge, "Wind power ramp event forecasting using a stochastic scenario generation method," *IEEE Trans. Sustain. Energy*, vol. 6, no. 2, pp. 422–433, Apr. 2015.
[6] M. Cui, D. Ke, Y. Sun, D. Gan, J. Zhang, and B.-M. Hodge, "A scenario generation method for wind power ramp events forecasting," in *Proc. IEEE Power Energy Soc. Gen. Meeting*, Denver, CO, USA, 2015.
[7] R. Sevlian and R. Rajagopal, "Detection and statistics of wind power ramps," *IEEE Trans. Power Syst.*, vol. 28, no. 4, pp. 3610–3620, Nov. 2013.
[8] R. Sevlian and R. Rajagopal, "Wind power ramps: Detection and statistics," in *Proc. IEEE Power Energy Soc. Gen. Meeting*, San Diego, CA, USA, 2012, pp. 1–8.
[9] E. H. Bristol, "Swinging door trending: Adaptive trend recording?" in *Proc. ISA Nat. Conf.*, 1990, pp. 749–756.
[10] A. Florita, B. M. Hodge, and K. Orwig, "Identifying wind and solar ramping events," in *Proc. IEEE 5th Green Technol. Conf.*, Denver, CO, USA, 2013, pp. 4–5.
[11] J. Zhang, A. Florita, B.-M. Hodge, and J. Freedman, "Ramp forecasting performance from improved short-term wind power forecasting," presented at the ASME Int. Design Eng. Tech. Conf. Comput. Inf. Eng. Conf. (IDETC/CIE'14), Buffalo, NY, USA, Aug. 17–20, 2014.
[12] Y. V. Makarov, C. Loutan, J. Ma, and P. Mello, "Operational impacts of wind generation on California power systems," *IEEE Trans. Power Syst.*, vol. 24, no. 2, pp. 1039–1050, May 2009.
[13] J. Ma, Y. V. Makarov, C. Loutan, and Z. Xie, "Impact of wind and solar generation on the California ISO's intra-hour balancing needs," in *Proc. IEEE Power Energy Soc. Gen. Meeting*, San Diego, CA, USA, 2011, pp. 1–6.
[14] J. Ma, S. Lu, P. V. Etingov, and Y. V. Makarov, "Evaluating the impact of solar generation on balancing requirements in Southern Nevada System," in *Proc. IEEE Power Energy Soc. Gen. Meeting*, San Diego, CA, USA, 2012, pp. 1–7.
[15] J. Ma, S. Lu, R. P. Hafen, P. V. Etingov, Y. V. Makarov, and V. Chadliev, "The impact of solar photovoltaic generation on balancing requirements in the Southern Nevada System," in *Proc. Transm. Distrib. Conf. Expo.*, Orlando, FL, USA, 2012, pp. 1–9.
[16] D. C. Barr, "The use of a data historian to extend plant life," in *Proc. Int. Conf. Life Manage. Power Plants*, Edinburgh, U.K., Dec. 12–14, 1994, pp. 35–39.
[17] M. Cui, J. Zhang, A. R. Florita, B.-M. Hodge, D. Ke, and Y. Sun, "An optimized swinging door algorithm for wind power ramp event detection," in *Proc. IEEE Power Energy Soc. Gen. Meeting*, Denver, CO, USA, 2015.
[18] C. W. Potter, E. Grimit, and B. Nijssen, "Potential benefits of a dedicated probabilistic rapid ramp event forecast tool," in *Proc. IEEE Power Syst. Conf. Expo.(PSCE)*, Seattle, WA, USA, 2009, pp. 1–5.
[19] C. Kamath, "Understanding wind ramp events through analysis of historical data," in *Proc. Transm. Distrib. Conf. Expo.*, New Orleans, LA, USA, 2010, pp. 1–6.
[20] C. Kamath, "Associating weather conditions with ramp events in wind power generation," in *Proc. Power Syst. Conf. Expo. (PSCE)*, Phoenix, AZ, USA, 2011, pp. 1–8.
[21] C. Ferreira, J. Gama, L. Matias, A. Botterud, and J. Wang, "A survey on wind power RAMP forecasting," Argonne Nat. Lab. (ANL), DuPage County, IL, USA, Tech. Rep. ANL/DIS-10-13, Dec. 2010.
[22] E. Ela and M. O'Malley, "Study the variability and uncertainty impacts of variable generation at multiple timescales," *IEEE Trans. Power Syst.*, vol. 27, no. 3, pp. 1324–1333, Aug. 2012.
[23] P. J. Roebber, "Visualizing multiple measures of forecast quality," *Weather Forecasting*, vol. 24, no. 2, pp. 601–608, Apr. 2009.
[24] M. Cui, J. Zhang, A. R. Florita, B.-M. Hodge, D. Ke, and Y. Sun, "Solar power ramp events detection using an optimized swinging door algorithm," in *Proc. ASME Int. Design Eng. Tech. Conf. Comput. Inf. Eng. Conf.*, Boston, MA, USA, 2015.
[25] L. Xu and D. Tretheway, "Flexible ramping products," California Independent System Operator (ISO), Folsom, CA, USA, 2012.
[26] N. Navid and G. Rosenwald, "Market solutions for managing ramp flexibility with high penetration of renewable resource," *IEEE Trans. Sustain. Energy*, vol. 3, no. 4, pp. 784–790, Oct. 2012.

Mingjian Cui (S'12) received the B.E. degree in electrical engineering and automation from Wuhan University, Wuhan, China, in 2010, where he is currently working toward the Ph.D. degree in electrical engineering.

Recently, he was a Visiting Scholar at the Transmission and Grid Integration Group (TGIG), National Renewable Energy Laboratory (NREL), Golden, CO, USA. His research interests include wind power ramp events forecasting, power system control, and big data analytics.

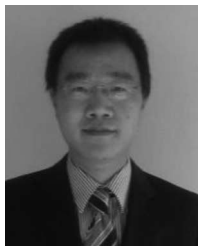

Jie Zhang (M'13–SM'15) received the B.S. and M.S. degrees from Huazhong University of Science and Technology, Wuhan, China, and the Ph.D. degree from the Rensselaer Polytechnic Institute, Troy, NY, USA, all in mechanical engineering, in 2006, 2008, and 2012, respectively.

He is currently a Research Engineer with the Transmission and Grid Integration Group (TGIG), National Renewable Energy Laboratory (NREL), Golden, CO, USA. His research interests include multidisciplinary design optimization, complex engineered systems, big data analytics, wind energy, renewable integration, energy systems modeling, and simulation.

Anthony R. Florita (M'13) received the B.S. degree in architectural engineering from the University of Wyoming, Laramie, WY, USA, in 2003, and the M.S. degree in mechanical engineering from the University of Nebraska, Lincoln, NE, USA, in 2007. Currently he is pursuing the Ph.D. degree in architectural engineering from the University of Colorado, Boulder, CO, USA.

He is currently a Research Engineer with the Transmission and Grid Integration Group (TGIG), National Renewable Energy Laboratory (NREL), Golden, CO, USA. His research interests include multidisciplinary design optimization, complex engineered systems, big data analytics, wind energy, renewable integration, energy systems modeling, and simulation.

Bri-Mathias Hodge (M'10) received the B.S. degree in chemical engineering from Carnegie Mellon University, Pittsburgh, PA, USA, in 2004, the M.S. degree from the Process Design and Systems Engineering Laboratory, Åbo Akademi University, Turku, Finland, in 2005, and the Ph.D. degree in chemical engineering from Purdue University, West Lafayette, IN, USA, in 2010.

He is currently a Section Supervisor of System Planning and Reliability with the Transmission and Grid Integration Group (TGIG) and a Senior Engineer with the National Renewable Energy Laboratory (NREL), Golden, CO, USA. His research interests include energy systems modeling, simulation, optimization, and wind power forecasting.

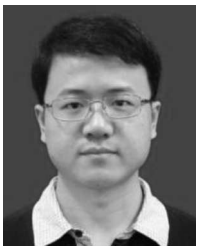

Deping Ke received the B.S. and M.S. degrees from Huazhong University of Science and Technology, Wuhan, China, and the Ph.D. degree from Hong Kong Polytechnic University, Kowloon, Hong Kong, all in electrical engineering, in 2005, 2007, and 2012, respectively.

Currently, he is a Lecturer with the School of Electrical Engineering, Wuhan University, Wuhan, China. His research interests include power system dynamics and control.

Yuanzhang Sun (M'99–SM'01) received the B.S. degree from Wuhan University of Hydro and Electrical Engineering, Wuhan, China, the M.S. degree from the Electric Power Research Institute (EPRI), Beijing, China, and the Ph.D. degree from Tsinghua University, Beijing, China, all in electrical engineering, in 1978, 1982 and 1988, respectively.

Currently, he is a Professor with the School of Electrical Engineering, Wuhan University, Wuhan, China, and a Chair Professor with the Department of Electrical Engineering and Vice Director of the State Key Lab of Power System Control and Simulation, Tsinghua University. His research interests include power system dynamics and control, wind power, voltage stability and control, and reliability.